

High-Throughput Detection and Sizing of Individual Low-Index Nanoparticles and Viruses for Pathogen Identification

G. G. Daaboul,[†] A. Yurt,[‡] X. Zhang,[†] G. M. Hwang,^{||} B. B. Goldberg,^{†,§,⊥} and M. S. Ünlü^{*,†,§,⊥}

[†]Department of Biomedical Engineering, Boston University, 44 Cummington Street, fourth floor, Boston, Massachusetts 02215, United States, [‡]Division of Materials Science and Engineering, Boston University, 15 Saint Mary's Street Brookline, Massachusetts 02446, United States, [§]Department of Electrical and Computer Engineering, Boston University, 8 St. Mary's Street, Room 324, Boston, Massachusetts 02215, United States, ^{||}The MITRE Corporation, McLean, Virginia 22102, United States, and [⊥]Physics Department, Boston University, 590 Commonwealth Avenue, Boston, Massachusetts 02215, United States

ABSTRACT Rapid, chip-scale, and cost-effective single particle detection of biological agents is of great importance to human health and national security. We report real-time, high-throughput detection and sizing of individual, low-index polystyrene nanoparticles and H1N1 virus. Our widefield, common path interferometer detects nanoparticles and viruses over a very large sensing area, orders of magnitude larger than competing techniques. We demonstrate nanoparticle detection and sizing down to 70 nm in diameter. We clearly size discriminate nanoparticles with diameters of 70, 100, 150, and 200 nm. We also demonstrate detection and size characterization of hundreds of individual H1N1 viruses in a single experiment.

KEYWORDS Biosensing, virus detection, interferometry, LED interferometry, scattering, interferometric imaging, high-throughput

Nanoparticle detection and characterization play a critical role in human health through the detection of air pollutants and pathogens. Inhalation of nanoparticle pollutants can cause inflammatory response in the lungs and spread to other organs.¹ Nanoscale pathogens cause many human diseases and viruses in particular have created widespread concern in the past decade as biowarfare agents.^{2–4} Speed and portability of sensor platforms are critical factors necessary to stop the spread of pandemics like influenza. While several techniques have shown the capability of detecting single nanoparticles or viruses, their widespread use has been hampered due to high-cost instrumentation and bulkiness.^{5,6} Recently, much effort has been spent developing resonant photonic devices to reduce complexity and increase sensitivity.^{7–10} The detection of single binding events of influenza A and polystyrene bead particles down to 60 nm has been demonstrated using a whispering gallery mode (WGM) device.^{10–12} Yet these devices cannot distinguish the size of individual nanoparticles when measuring an unknown, heterogeneous mixture and, like all discrete resonant photonic devices, tend to be prone to environmental noise.^{12,13}

Most biological agents are difficult to detect optically because they are small, weakly interact with photons, and have low index contrast to the surrounding medium.¹⁴ In

order to increase the interaction of light with particle, high NA objectives or resonant structures are commonly used. In classical theory, the interaction of a particle with light can be understood via induced dipoles on a nonabsorbing particle. In the quasi-static theory, the strength of the induced dipole is proportional to polarizability of the small particle

$$\alpha = 4\pi\epsilon_0 r^3 \frac{\epsilon_p - \epsilon_m}{\epsilon_p + 2\epsilon_m}$$

where r is the particle radius and ϵ_p and ϵ_m are the particle and surrounding medium permittivity, respectively.¹⁵ Detection techniques which depend on the scattered intensity have a detector signal given as $I \propto |E_s|^2$ which scales with $|\alpha|^2 \propto R^6$. The large variability in size of biological agents limits the use of pure elastic scattering since the signal vanishes below the shot-noise limit for small particles. On the other hand, interferometric methods have a signal at the detector is given as

$$I \propto |E_s + E_r|^2 = |E_s|^2 + |E_r|^2 + 2\text{Re}(E_r E_s^*)$$

which mix a strong reference with weak scattered fields from the particle. For small particles, the first term is small relative to the other two, and the second term is a readily subtracted offset. The detector signal is multiplied by the reference field and scales proportional to $|\alpha| \propto R^3$. The amplitude and phase of the reference beam can also be

* To whom correspondence should be addressed: College of Engineering, 8 St. Mary's St., Boston, MA 02215; tel, +1 617 353 5067; fax, +1 617 353 6440; e-mail, selim@bu.edu.

Received for review: 09/11/2010

Published on Web: 00/00/0000

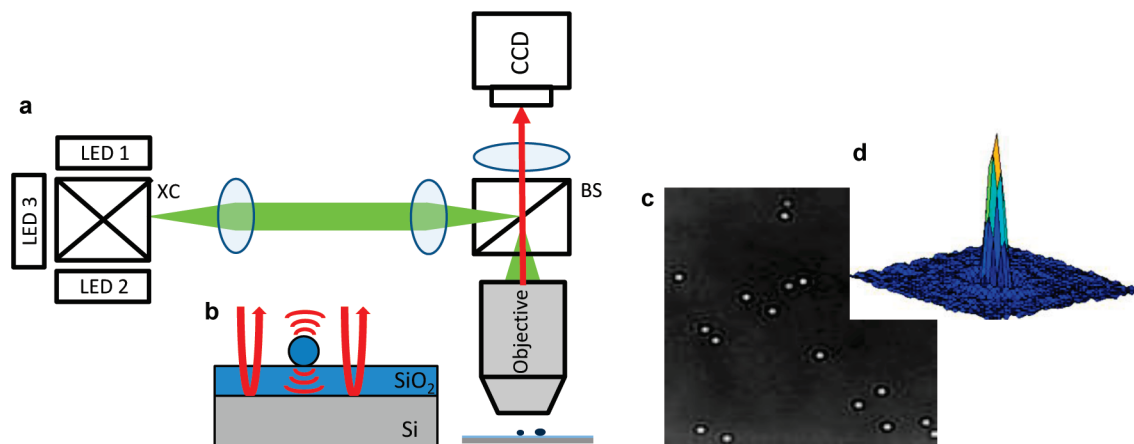


FIGURE 1. Experimental setup. (a) Schematic of the optical setup: XC, x-cube used to combine the beams of the different LEDs; BS, beam splitter. (b) Illustrates the layered substrate and shows the optical paths that produced the interference signal. (c) An image of 150 nm diameter beads at a wavelength of 635 nm. (d) Response of a 150 nm diameter bead shown in (c).

externally adjusted to further improve the SNR of detection.¹⁷ Thus interferometric detection improves both dynamic range and sensitivity to small particles compared to pure scattering techniques. However, the drawback of utilizing an external reference mirror is that such systems require very stable and sensitive optical setups, since even small mechanical vibrations or index fluctuations in the optical path of either signal or reference beam cause uncertainty in the phase relation between the reference and scattered fields, yielding erroneous results when sizing of nanoparticles is of interest.¹⁸ To date, no interferometric technique has been shown to demonstrate sizing small nanoparticles with high-throughput and single particle sensitivity.

In this Letter, we demonstrate an interferometric technique capable of detecting and size characterizing nanoparticles on a high throughput and robust widefield imaging platform. We overcome limitations of conventional interferometric techniques by using a common-path configuration enabled by a layered substrate that can be optimized for various particle size ranges of interest. The layered substrate consists of a thermally grown silicon dioxide layer on a silicon substrate providing a smooth, uniform, and flat layer structure with precise thickness control. The oxide provides a very stable uncommon path, so interference of light reflected from the top oxide surface and the oxide/silicon interface results in a well characterized response for any given wavelength of light for each particle size. Our technique improves over existent nanoparticle imaging approaches by eliminating active optical and scanning elements obviating the need for complex hardware and optical setup. The advantage of using a common-path interferometric configuration on a layered substrate also allows the response to be tuned, significantly increasing SNR and permitting very large sensing areas to be simultaneously imaged. In this Letter we demonstrate detection and sizing of polystyrene particles with similar refractive index and size as viruses. We also present results on detecting and sizing individual H1N1 (A/PR/8/34) influenza.

Results. Interferometric Reflectance Imaging Sensor. Our technique is evolved from earlier work on a spectral reflectance imaging biosensor¹⁹ that utilizes a Si/SiO₂ substrate to optimize phase imaging in a widefield, common path interferometer for the real-time measurement of accumulated biomass in a microarray format. We extend the application of interferometric imaging on a layered substrate to high spatial resolution and maintain a relatively constant phase of the reflected incident light at high numerical aperture (NA) by using a thin oxide top layer to minimize the optical path difference at different angles.

Figure 1 shows a schematic of an imaging interferometer with a 50× NA = 0.8 objective and a three LED illumination source with central wavelengths of 450, 525, and 635 nm in Kohler illumination configuration. When nanoparticles are immobilized on the surface, the interference of the scattered and back reflected light gives a quantifiable signal that is used to detect and size the particles on the surface (Figure 1b–d). The interferometric response of nanoparticles on the surface can be captured simultaneously over a large area, effectively limited only by the CCD size and imaging optics and positioning system. The interferometric intensity image from a small subregion of the sensor surface is shown in Figure 1c, with the response from a single nanoparticle shown in Figure 1d.

Interferometric images are acquired at multiple wavelengths, and an automated image processing algorithm written in MATLAB is used to search for local maxima or minima above the image noise level that fall within the width of the point spread function of the system. This discriminates against particle aggregation and larger impurities such as dust particles. The combined response at different wavelengths for each peak is normalized by the background intensity in the vicinity of each nanoparticle and then fit to a forward model to determine the individual particle sizes. We term this technique IRIS for interferometric reflectance imaging sensor.

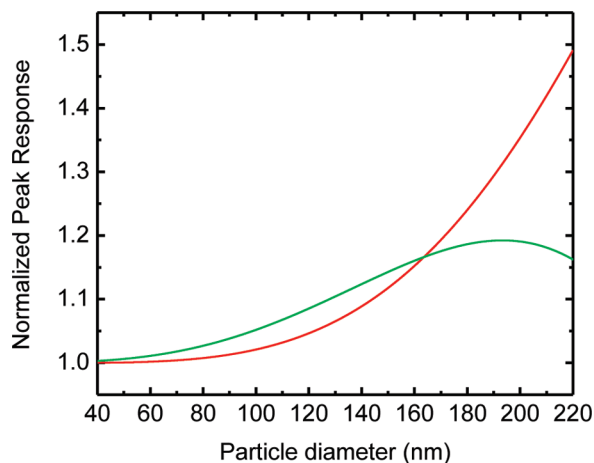


FIGURE 2. Interference response. Theoretical interference response vs particle size for 525 and 635 nm central wavelength LEDs.

In the forward model, we assume particles are Rayleigh scatterers on top of the given multilayered media. The particles interact with both the incident field and the reflected field from the layered media. Once the scattered field is obtained in the far-field regime, the image of the particles through the telescopic imaging system is calculated using Angular Spectrum Representation where the particles are modeled as dipoles.²² (See methods for details.) The interferometric signal is modified by the proximity of the particle to the layered substrate, yielding a mixture of the simple sinusoidal response of an added uniform layer and the R^3 dependence of a particle in free space. This approach of using a layered substrate with multiple wavelength illumination allows real-time optimization of optical response for a given particle size range. Clearly, for each particle size range a set of optimized wavelengths would yield the highest size discrimination capability. Our technique relies on multiple wavelengths to determine the precise thickness of the oxide layer in the vicinity of the particles. For a particular oxide thickness and illumination wavelength, reflectivity modified by a particle on the surface has a very specific functional dependence on the size of the particle, and therefore the size can be determined using the intensity images at a single wavelength. As an example, the normalized peak response as a function of particle size on a 113 nm thick SiO_2 slab is given in Figure 2 for two different wavelengths. In this plot, a higher slope of the curve corresponds to better size discrimination ability. Consequently, for particles with diameter of 100 nm (or smaller), the green LED (525 nm) provides higher detection sensitivity (response) compared to the red LED (630 nm). On the other hand, for the particle sizes at around 200 nm diameter, the response of a green LED becomes double valued and cannot be used to determine the size of the particles. In this case, the red LED response provides sizing resolution. As this example illustrates, we can analyze the images acquired with multiple color illumination sources and utilize a different color image for each particle size range based on the

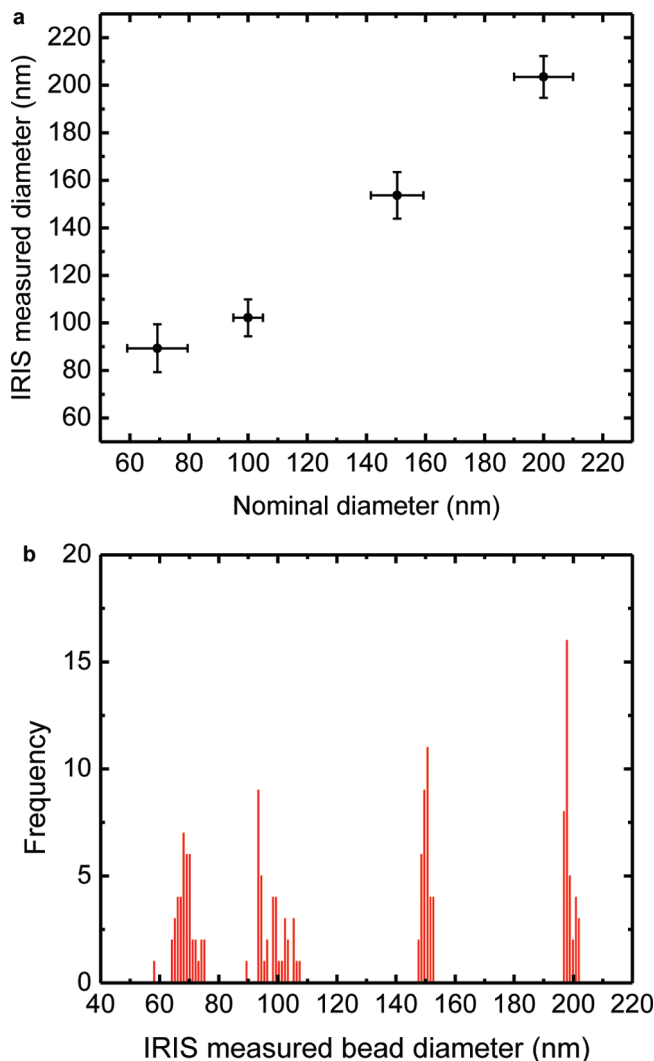


FIGURE 3. Single particle sizing and error analysis: (a) IRIS measured particle diameter vs nominal diameter with error bars indicating size distribution; (b) size distribution of consecutive measurement of a single particle.

observed contrast for particles in the field of view. This analysis is not computationally intensive and can be done in real time.

Nanoparticle Sizing. Polystyrene beads of nominal diameters of 70 nm, 100 nm, 150 nm and 200 nm are immobilized on the SiO_2/Si substrate with a 113 nm thick oxide layer (see Methods). The peak response values for each nanoparticle in the image is normalized by the background intensity in its local vicinity and the normalized peak response values are fit to the forward model prediction. For this paper, we use two wavelengths and minimize sizing error with respect to the combined responses. Figure 3 demonstrates that IRIS can easily detect and size nanoparticles from 100 to 200 nm diameter accurately, and although 70 nm particles are overestimated in size, we believe this is due to a focusing error, discussed below. The graph shows that the measured mean is $\sim 2\%$ deviated from the nominal mean reported by the manufacturer and the measured

standard deviations of the bead distributions are 10.1, 7.8, 9.8, and 8.8 nm for 70, 100, 150, and 200 nm diameter particles, respectively. The accuracy of sizing is dependent on the validity of the parameters in the forward model and experimental error. The formulations of the forward model's parameters (i.e., material dispersion) are well-known for the materials used; however, the illumination profile for the different LEDs cannot be exactly known and similarly the coherence function have to be estimated. In addition, the response curve is calculated based on a fixed oxide thickness, and while we believe this to be accurate to within a few nanometers, deviations between substrates or across the same chip will cause a small change in the predicted response. IRIS is also a multiple wavelength reflectometer which can correct for any local fluctuations in oxide thickness or dispersion across the substrate's surface as described in detail elsewhere.¹⁹

To determine the repeatability and precision of the sizing measurements, we took 35 consecutive images of the same substrate area and determined the standard deviation of the measured size of a single bead. Figure 3b shows the measured size distribution of a single bead, whose width is due to the system noise comprised of vibrations, stage drift, and electronic noise from the CCD camera which is dominated by detector shot noise. The noise is plotted for each bead size since it depends on the slope of the response curve which itself varies as a function of particle size. The standard deviation for the repeated measurements are 3.2, 4.7, 1.3, and 1.5 nm for 70, 100, 150, and 200 nm diameter beads, respectively. The standard deviation for the 150 and 200 nm diameter beads is at the shot-noise limit which could be further improved by increasing the incident power or averaging additional frames. The error for the 70 and 100 nm diameter beads is higher due to a slow vertical drift of the stage that is evident in time traces (not shown). This optical axis drift demonstrates the sensitivity to the focal plane position (see Supplementary Figure 1 found in the Supporting Information) and is most challenging for 70 nm particles and smaller since manual focusing is more difficult. Future corrections could be done through placing a high contrast fiducial mark on the surface to locally optimize the focus or performing z-scans and fitting the oscillation in phase to the forward model at peak response.

Influenza Detection and Sizing. H1N1 influenza virus was immobilized on the surface to demonstrate pathogen detection and sizing (see Methods). The IRIS intensity image is shown in Figure 4a and a scanning electron microscope (SEM) image of the same region (Figure 4b) confirms the immobilization of single virions. A comparison of the SEM and IRIS images shows a one-to-one correspondence between each virion in the SEM and each particle in the IRIS image. SEM measurements of single viruses yield a mean diameter of 120 nm and a range from 90 to 160 nm (see SEM inset). The viruses were sized using IRIS with the green LED and forward model as discussed above, with the result-

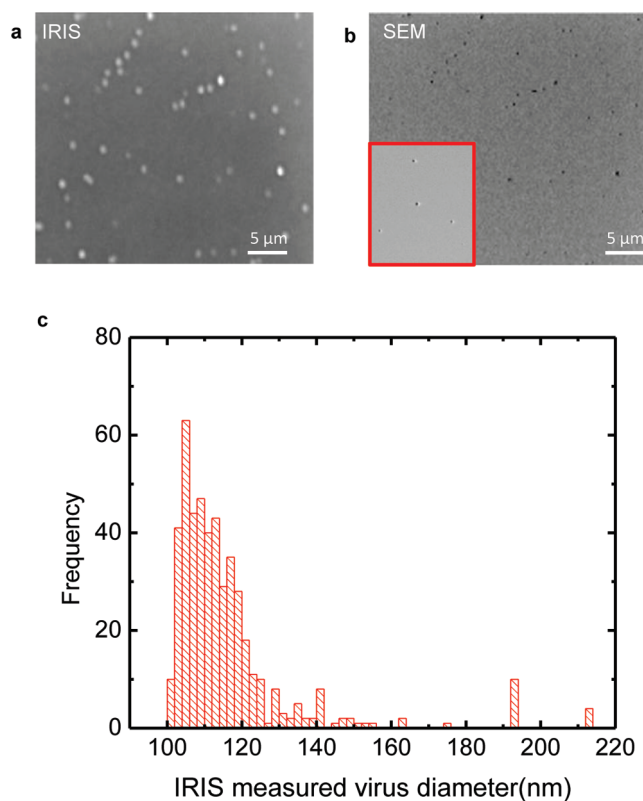


FIGURE 4. H1N1 virus detection and sizing: (a) IRIS image of immobilized virus on the surface with the same field of view as the SEM image; (b) SEM image of immobilized virus on the surface; (c) measured size distribution of immobilized virus using IRIS.

ing distribution shown in Figure 4c. The IRIS measured mean and size distribution is 116 and 17 nm, respectively, in agreement with reported diameters in the literature²⁰ and SEM measurements on this sample.

Conclusion. Detection and sizing of individual nanoparticles on a high-throughput, low-cost, and compact platform can have a wide impact on biosensing and monitoring environmental and health hazards. Two figures of merit used to describe any biosensor are sensitivity and specificity. Single pathogen detection represents the ultimate sensitivity limit which our method provides. However, high sensitivity can lead to false positives due to unspecific binding to the probe. One way to improve on the specificity of the sensor is by using multiple probes that are specific for different moieties on the same target. The parallel sensing nature of this technique allows for multiplexed detection of pathogens by functionalizing different sensing regions against different moieties and targets. When multiple probes and control are present and a sufficient amount of particles captured, traditional statistical analysis can be used to determine if a certain pathogen is present. When few pathogens are captured on the surface, conventional statistical tools cannot be used to draw a conclusion. Additional information on the detected particles can dramatically improve specificity. Existing methods based on high-Q microresonators are capable of detecting and sizing single nanoparticles provided

that only a single binding event of particles occurs at a given time. In addition to the low-throughput bottleneck, the challenges are yet to be addressed regarding measuring pathogens in complex solutions where a variety of pathogen sizes and other biomolecules which shift the resonance are present. Our widefield interferometric imaging method demonstrates detection and accurate sizing of a range of nanoparticles and is shown to be effective for single virus detection. Unlike discrete resonant devices, our platform has sensitivity and response that are independent of the binding location on the sensor surface, making it easy to detect and size an individual particle bound anywhere on the entire sensor surface, effectively yielding 10^5 – 10^6 parallel sensing elements. We also have demonstrated size discrimination using H1N1 virus and propose to further improve specificity by incorporating shape recognition. The IRIS technique probes the polarizability of the nanoparticles on the surface which is dependent on the particle size, refractive index, and geometry and orientation. Using the quasi-static approximation for ellipsoid particles the induced dipole moment of the particle in each axis can be estimated using a polarized scattering measurement technique. If the permittivity values of the particle and surrounding medium are known, then several consecutive measurements with different illumination polarization vectors can reveal the size, aspect ratio, and orientation of the particle using the IRIS setup. In our future work we plan to implement orientation and shape recognition by introducing simple polarization optics elements in the optical setup. (For details see Supporting Information.)

Acknowledgment. This work was partially funded by Army Research Laboratories (6) under the Contracts No. W911NF-06-2-0040, the Smart Lighting Engineering Research Center (EEC-0812056), and The MITRE Corporation under Research Agreement Numbers 79952, 80814, and 81646. Approved for Public Release, Case # 10-3211. G.D. would like to acknowledge Ronen Adato for his help with SEM imaging and Priscilla Renda for fruitful discussions and help in experimental design.

Supporting Information Available. Detailed experimental procedures and modeling for size and shape discrimination. This material is available free of charge via the Internet at <http://pubs.acs.org>.

REFERENCES AND NOTES

- (1) Somers, C. M.; McCarry, B. E.; Malek, F.; Quinn, J. S. Reduction of particulate air pollution lowers the risk of heritable mutations in mice. *Science* **2004**, *304*, 1008–1010.
- (2) Anderson, B.; Friedman, H.; Bendinelli, M. *Microorganisms and Bioterrorism*; Springer: New York, 2009.
- (3) Laver, G.; Garman, E. Virology. The origin and control of pandemic influenza. *Science* **2001**, *293*, 1776–1777.
- (4) Krug, R. M. The potential use of influenza virus as an agent for bioterrorism. *Antiviral Res.* **2003**, *57*, 147–150.
- (5) Kukura, P.; et al. High-speed nanoscopic tracking of the position and orientation of a single virus. *Nat. Methods* **2009**, *6*, 923–928.
- (6) Szymanski, W. W.; Nagy, A.; Czitrovsky, A.; Jani, P. A new method for the simultaneous measurement of aerosol particle size, complex refractive index and particle density. *Meas. Sci. Technol.* **2002**, *13*, 303–307.
- (7) Armani, A. M.; Kulkarni, R. P.; Fraser, S. E.; Flagan, R. C.; Vahala, K. J. Label-free, single-molecule detection with optical microcavities. *Science* **2007**, *317*, 783–787.
- (8) Armani, D. K.; Kippenberg, T. J.; Spillane, S. M.; Vahala, K. J. Ultra-high-Q toroid microcavity on a chip. *Nature* **2003**, *421*, 925–928.
- (9) Kippenberg, T. J.; Spillane, S. M.; Armani, D. K.; Vahala, K. J. Fabrication and coupling to planar high-Q silica disk microcavities. *Appl. Phys. Lett.* **2003**, *83*, 797–799.
- (10) Vollmer, F.; Arnold, S. Whispering-gallery-mode biosensing: label-free detection down to single molecules. *Nat. Methods* **2008**, *5*, 591–596.
- (11) Vollmer, F.; Arnold, S.; Keng, D. Single virus detection from the reactive shift of a whispering-gallery mode. *Proc. Natl. Acad. Sci. U.S.A.* **2008**, *105*, 20701–20704.
- (12) Zhu, J.; et al. On-chip single nanoparticle detection and sizing by mode splitting in an ultrahigh-Q microresonator. *Nat. Photonics*, *4*, 46–49.
- (13) Chantada, L.; Nikolaev, N. I.; Ivanov, A. L.; Borri, P.; Langbein, W. Optical resonances in microcylinders: response to perturbations for biosensing. *J. Opt. Soc. Am. B* **2008**, *25*, 1312–1321.
- (14) Mahy, B. *Microbiology and Microbial Infections*, 9th ed.; A Hodder Arnold Publication: London, 1998.
- (15) Bohren, C.; Huffman, D. *Absorption and Scattering of Light by Small Particles*; Wiley-VCH: New York, 1998.
- (16) Colpin, Y.; Swan, A.; Zvyagin, A. V.; Plakhotnik, T. Imaging and sizing of diamond nanoparticles. *Opt. Lett.* **2006**, *31*, 625–627.
- (17) Ignatovich, F. V.; Novotny, L. Real-time and background-free detection of nanoscale particles. *Phys. Rev. Lett.* **2006**, *96*, +.
- (18) Mitra, A.; Deutsch, B.; Ignatovich, F.; Dykes, C.; Novotny, L. Nanofluidic Detection of Single Viruses and Nanoparticles. *ACS Nano* **2010**, *4*, 1305–1312.
- (19) Ozkumur, E.; et al. Label-free and dynamic detection of biomolecular interactions for high-throughput microarray applications. *Proc. Natl. Acad. Sci. U.S.A.* **2008**, *105*, 7988–7992.
- (20) Wrigley, N. G. Electron microscopy of influenza virus. *Br. Med. Bull.* **1979**, *35*, 35–38.
- (21) Mertz, J. C. *Introduction to Optical Microscopy*; Roberts and Company Publishers: Greenwood Village, CO, 2009.
- (22) Novotny, L.; Hecht, B. *Principles of Nano-Optics*; Cambridge University Press: Cambridge, 2006.